An Investigation of a Dark Sector Interaction Model to Solve the Hubble Tension

Angela Zhou

Magee Secondary School

Abstract

The current standard cosmology model is the ΛCDM model, encodes independent, time-dependent evolution of baryons, radiation, and cold dark matter, as well as time-independent dark energy in the form of a cosmological constant that accelerates the expansion of the universe. Current measurements of the Hubble constant from model-dependent sources demonstrate statistical significances of over 4σ from model-independent measurements, suggesting that physics beyond ΛCDM exists.

In this project, the ΛCDM model was changed in order to reduce this Hubble constant disagreement. We propose the Interacting Dark Sector (IDS) model, which introduces decay-type interactions between cold dark matter and dark energy; this decay is proportional to the CDM density parameter but is restricted at early, CDM-dense times to preserve present-day CDM density.

Then, a Markov chain Monte Carlo sampling algorithm was used to determine the probability distributions and best-fit values for different density parameters and for the Hubble Rate. The results for datasets with Riess et al. (2019) H_0 suggest a relationship between decaying dark energy and reduced Hubble tension; however, the results generally suggest that IDS is highly unlikely to solve the Hubble tension given our current understanding of the universe.

1 Introduction

1.1 Motivation

1.1.1 Historical Background

Einstein's original formulation of his field equations included a dark energy term in the form of a cosmological constant Λ to allow for a flat a static universe. This addition was quite arbitrary, but did not violate any physical laws because Λ, being a constant, did not affect energy conservation. Hubble's discovery of the universe's expansion prompted Einstein to remove Λ from his field equations, going as far as to call the original addition of Λ his "biggest blunder".

The development of a dark matter theory occurred generally independently from that of a dark energy theory. Throughout the 20th century, observation evidence from galaxy rotation curves to the mass of the Oort cloud consistently pointed to the existence of some form of matter which does not interact electromagnetically, thus the name *dark* matter. Multiple theories about the size and velocity of dark matter were proposed and explored: low-mass, relativistic "hot dark matter"; high-mass, nonrelativistic "cold dark matter"; and "warm dark matter", which has properties that lie between those of the other two. In the end, cold dark matter (CDM) prevailed; it is currently widely-accepted as the most likely form of dark matter and is the form of dark matter present in the ΛCDM model. For decades, Λ was assumed to be 0 by most scientists. The idea of a nonzero

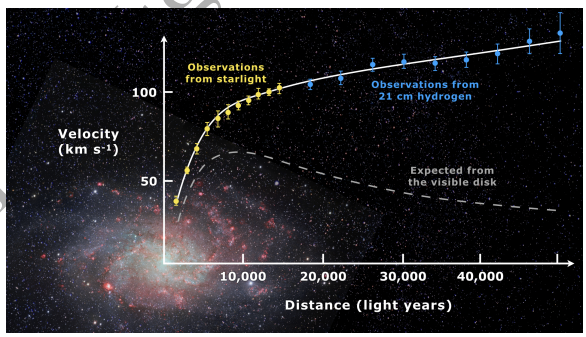

Figure 1: Graph of the observed rotation velocities at different radii in Messier 33 (Triangulum Galaxy) vs. predicted rotation velocities with only visible matter - this discrepancy suggests the existence of dark matter
Credit: Mario De Leo / CC BY-SA

Λ once again arose in 1998, when observations of distances to high redshift

type Ia supernovae determined that their measured distances are shorter than those predicted [17], leading to the idea that $\dot{a}$ is increasing, which required the re-addition of Λ. While there had been no evidence of whether Λ was actually constant, it was generally accepted to be so and the ΛCDM model quickly gained status-quo status.

Since then, as the amount of cosmological data has increased, the ΛCDM model has been supported numerous times, mostly through indirect measurements of early-universe density parameters and their extrapolated present-day density parameters. These early-universe measurements often come from time of photon decoupling, the time approximately $370,000$ years after the big bang and at redshift $z = 1090$ when photons first started to be able to travel freely, independent of interference from baryons. Cosmic microwave background (CMB) patterns originate from the photons that started freely travelling at photon decoupling.

CMB power spectra and gravitational lensing measurements from the NASA Wilkinson Microwave Anisotropy Probe (WMAP) [7] and the ESA Planck Satellite [11] are both well-supported by the ΛCDM model; in other words, cosmological density parameters predicted by the ΛCDM model in conjunction with WMAP and Planck data are within ranges specified by direct measurements.

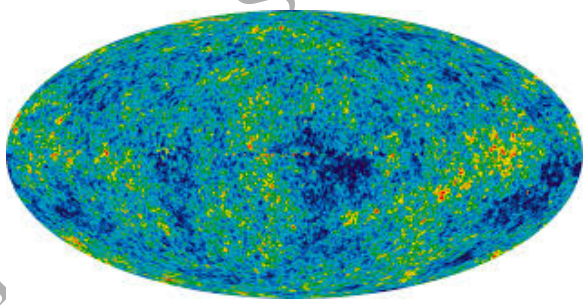

Figure 2: CMB map from the NASA Wilkinson Microwave Anisotropy Probe, 2010
Credit: NASA WMAP

Furthermore, Planck constraints from ΛCDM describe redshift and cosmological distance datapoints from baryon acoustic oscillations (BAO), patterns in baryon density caused by matter-radiation interactions in the early universe measured from 1.5 million galaxies in the redshift range $0.2 < z < 0.7$, to within 1σ [1]. BAO measures properties of the sound horizon at decoupling, at distance r_d, the

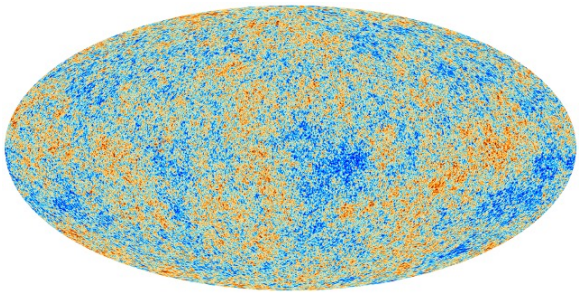

Figure 3: CMB map from the ESA Planck Satellite, 2018
Credit: ESA Planck Satellite

total distance sound has travelled since decoupling. Many other datasets that describe CMB, such as the South Pole Telescope Sunyarv-Zel'dovich (SPT-SZ) survey, which measures the amount of Inverse Compton Scattering distortion of CMB, fit ΛCDM well [2].

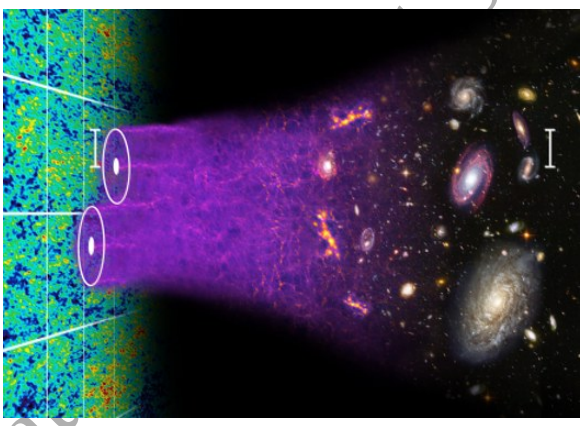

Figure 4: Illustration of baryon acoustic oscillations measurements from galaxies; distances between galaxies are directly related to CMB radiation patterns
Credit: Chris Blake and Sam Moorfield

1.1.2 Disagreements with ΛCDM

Despite its wide range of support, model-independent measurements of the Hubble rate disagree significantly with ΛCDM. Such measurements involve the computation of the Hubble rate using measured redshift and a local measurement of luminosity or angular diameter distance. The apparent magnitudes of Cepheid and Mira variables, pulsating stars that are known as *standard candles* due to

their well-defined period-luminosity relations, could be used to determine distances to their host galaxies. Gravitational lensing and masers could similarly be used to determine distances. The most well-known instance of local determination of the Hubble constant involved Cepheid variables and determined the Hubble rate to within 1.19% uncertainty as $H_0 = 74.03 \pm 1.42$ km s^{-1} Mpc^{-1}, 4.4σ away from 6.6 ± 1.5 km s^{-1} Mpc^{-1}, the value predicted by ΛCDM and Planck CMB [16]. Other methods of distance determination yielded similar Hubble rates of 73.3 ± 4.0 km s^{-1} Mpc^{-1} [8], $73.3^{+1.7}_{-1.8}$ km s^{-1} Mpc^{-1} [21], and 73.9 ± 3.0 km s^{-1} Mpc^{-1} [14].

These discrepancies strongly suggest that physics beyond ΛCDM exists.

1.2 Basic Theory of the Expanding Universe

In the static universe of special relativity, spacetime is described by the Minkowski metric, defined as

$$\eta_{\mu\nu} = \begin{pmatrix} -1 & 0 & 0 & 0 \\ 0 & 1 & 0 & 0 \\ 0 & 0 & 1 & 0 \\ 0 & 0 & 0 & 1 \end{pmatrix}. \tag{1}$$

This metric converts measurements to the invariant spacetime interval

$$ds^2 = -c^2 + x^2 + y^2 + z^2, \tag{2}$$

where c is set to 1 via change of units. In an expanding, isotropic universe, we adopt a comoving coordinate system, where the scale factor $a(t) = r(t)/r(0)$ is defined as the ratio between an arbitrary distance at time t and said distance at present $t = 0$. For a flat universe (which is well-supported by observations), the Minkowski metric, expressed in the comoving coordinate system, becomes the Friedmann-Robertson-Walker (FRW) metric,

$$g_{\mu\nu} = \begin{pmatrix} -1 & 0 & 0 & 0 \\ 0 & a^2(t) & 0 & 0 \\ 0 & 0 & a^2(t) & 0 \\ 0 & 0 & 0 & a^2(t) \end{pmatrix}. \tag{3}$$

For an isotropic universe approximated as a perfect fluid, the energy-momentum tensor is

$$T_{\mu\nu} = \begin{pmatrix} E & 0 & 0 & 0 \\ 0 & P & 0 & 0 \\ 0 & 0 & P & 0 \\ 0 & 0 & 0 & P \end{pmatrix}. \tag{4}$$

Einstein's field equations describe relationship between the universe's geometry in terms of the Ricci tensor $R_{\mu\nu}$ and the Ricci scalar $\mathcal{R}$ and the energy-momentum tensor, in curved spacetime:

$$R_{\mu\nu} - \frac{1}{2}\mathcal{R} = 8\pi G T_{\mu\nu}. \tag{5}$$

The 0-0 component of Einstein's Equation leads to the Friedmann Equation, which describes the time-dependency of the scale factor and density:

$$\left(\frac{\dot{a}}{a}\right)^2 = 8\pi G\rho. \tag{6}$$

Conservation of energy and momentum with the energy-momentum tensor and an equation of state $P = w\rho$ derived from statistical mechanics, where $w = 1/3$ for radiation and $w = 0$ for baryons and cold dark matter, yield differential equations for the time-evolution of baryon, radiation, and cold dark matter density:

$$\begin{aligned} \dot{\rho_b} + 3H\rho_b &= 0 \\ \dot{\rho_c} + 3H\rho_c &= 0 \\ \dot{\rho_r} + 4H\rho_r &= 0 \end{aligned} \tag{7}$$

Recent observations have suggested that the $\dot{a}$ is increasing, leading to the addition of a dark energy term in the form of a cosmological constant Λ. We define $\Omega_{b,c,r} = \rho_{b,c,r}/\rho_{\text{crit}}$, where $\rho_{\text{crit}} = 3H^2/8\pi G$ is the density necessary to maintain a static and flat universe. Similarly, we define $\Omega_\Lambda = \Lambda/3H^2$. These equations,

when combined with the differential equations, lead to

$$\begin{aligned}\frac{d\Omega_b}{da}+3\frac{\Omega_b}{a}&=0\\ \frac{d\Omega_c}{da}+3\frac{\Omega_c}{a}&=0\\ \frac{d\Omega_r}{da}+4\frac{\Omega_r}{a}&=0\\ \frac{d\Omega_\Lambda}{da}&=0,\end{aligned} \tag{8}$$

where present-day $\Omega_{b_0,c_0,r_0,\Lambda_0}$ satisfy

$$\frac{\Omega_b}{a^3}+\frac{\Omega_c}{a^3}+\frac{\Omega_r}{a^4}+\Omega_\Lambda=1. \tag{9}$$

This leads to a relationship between the present-day Hubble rate H_0 and the Hubble rate H at scale factor a,

$$H^2=H_0^2\left(\frac{\Omega_{b_0}}{a^3}+\frac{\Omega_{c_0}}{a^3}+\frac{\Omega_{r_0}}{a^4}+\Omega_{\Lambda_0}\right) \tag{10}$$

Since the Hubble constant is related to the scale factor a, observational masurements of the Hubble constant rely on the comoving distance $\chi(a)$, the distance light travels in an expanding coordinate system, of an observable object. All Hubble constant measurements are made indirectly by measuring three quantities related to $\chi(a)$: the redshift

$$z=\frac{\lambda_{\text{obs}}-\lambda_{\text{emit}}}{\lambda_{\text{obs}}}, \tag{11}$$

the angular diameter distance

$$d_A=\frac{\ell}{\theta}=a\chi(a), \tag{12}$$

and the luminosity distance

$$d_L=\sqrt{\frac{4\pi F}{L}}=\frac{\chi(a)}{a}. \tag{13}$$

1.2.1 Past Works

Much research has been done in the area of resolving Hubble rate tensions using modifications on the behaviours of dark matter and dark energy. The examples

listed in the forthcoming section only cover the three which are closest in topic to this project.

Many past works in this field involved altering the equation of state constant of dark energy and have provided strong support for dark energy density increasing over time [18]. von Marttens et al. (2019) [20] proposed and investigated a class of dark sector[1] interaction models. Miller (2019) [12] tested specific interaction models within said class of dark sector interactions that are strictly proportional to the total density of CDM and dark energy, and found that the density of CDM dominates this interaction. Furthermore, the results of Miller (2019) give strong support for dark sector interactions.

Much is still unknown about the properties of the dark sector. The purpose of this project is to investigate whether a new model that includes an interaction which is proportional to the amount of CDM at late times but decays to zero at early times would provide a better fit of data.

2 Methods

2.1 Overview

We seek to alter the dark energy density parameter differential equation of the ΛCDM model. By conservation of energy, any change in dark energy density must involve some sort of energy transfer to or from other species. In other words,

$$\frac{d\Omega_\Lambda}{da} + \frac{d\Omega_b}{da} + \frac{d\Omega_c}{da} + \frac{d\Omega_r}{da} = 0. \tag{14}$$

We determine that cold dark matter is the most logical candidate for this energy transfer, as baryons and radiation are relatively well-understood. Since they interact electromagnetically, some sort of energy transfer would likely be observable, making baryonic or radiative interactions highly unlikely. Our conservation of energy equation then becomes

$$-\frac{d\Omega_\Lambda}{da} = \frac{d\Omega_c}{da}. \tag{15}$$

[1] Dark matter and dark energy are together referred to as the *dark sector*.

We denote $Q = -d\Omega_\Lambda/da$. The evolution equations then become

$$\begin{aligned}
\frac{d\Omega_b}{da} &= -\frac{3\Omega_b}{a} \\
\frac{d\Omega_r}{da} &= -\frac{4\Omega_r}{a} \\
\frac{d\Omega_c}{da} &= -\frac{3\Omega_c}{a} + Q \\
\frac{d\Omega_\Lambda}{da} &= -Q.
\end{aligned} \tag{16}$$

Q was defined to be proportional to the density parameter Ω_c at recent times but drop for high values of Ω_c at early times. This situation is assumed in order to prevent the difference in the decay of Ω_c, which had a high value in the early universe, from drastically altering the current Ω_c value, as it is loosely constrained by observations. In order to achieve these bounds, a dimensionless proportionality parameter γ_0 was incorporated, and a function $\gamma(a)$ proportional γ_0 was defined. Furthermore, Q was defined to be proportional to this parameter, in the form

$$Q = \frac{3\Omega_c\gamma(a)}{a}. \tag{17}$$

The factor of $3/a$ multiplied to Q is quite arbitrary, but it was added to preserve the general form the Ω_c evolution equation.

A function that could describe the evolution of $\gamma(a)$ with time would depend on the times concerned. In this project, we integrate from the present time to times as early as recombination[2], $a = 1/1090$, to compare sample parameter values with early-universe data, a process detailed in Implementation. We want a function $\gamma(a)$ that is loosely defined to behave according to

$$\begin{cases}
\dfrac{\gamma(a)}{\gamma_0} \to 0 & \text{when } a \to 1/1090 \\
\dfrac{\gamma(a)}{\gamma_0} \to 1 & \text{otherwise.}
\end{cases} \tag{18}$$

One such function is defined and named the Interacting Dark Sector (IDS)

[2]BAO and CMB data originate from recombination, while HST and Supernovae data describe somewhat later times, albeit still in the early universe.

model. Q and $\gamma(a)$ of the IDS model behave according to

$$\begin{aligned} \gamma(a) &= \frac{1+\tanh\frac{\Omega_c}{\Omega_{c_1}}}{2} \\ Q &= \frac{3\Omega_c\left(1+\tanh\frac{\Omega_c}{\Omega_{c_1}}\right)}{2a} \end{aligned} \tag{19}$$

Here, Ω_{c_1} is the density parameter at some constant scale factor a_1 between the present time and recombination. Since γ_0 is very small, to reduce computation cost, we approximate $\Omega_c/\Omega_{c_1} \approx a_1^3/a^3$, the expression given by the ΛCDM model. Therefore,

$$Q = \frac{3\Omega_c\left(1+\tanh\frac{a_1^3}{a^3}\right)}{2a}. \tag{20}$$

We let $a_1 = 1090^{-3/2}$. This value of a_1 would allow Q to approach 0 only at values close to $a = 1/1090$. This can be seen in Figure 5, a log-log graph of $\gamma(a)/\gamma_0$ vs. a.

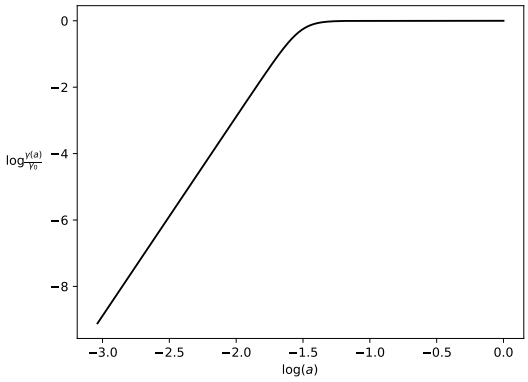

Figure 5: Graph of $\log(\gamma(a)/\gamma_0)$ vs. $\log(a)$ with IDS

We define

$$\Omega_{\text{tot}} \equiv \Omega_b + \Omega_c + \Omega_r + \Omega_\Lambda = \frac{H^2}{H_0^2}. \tag{21}$$

To get a better idea of how much Q affects the evolution of density parameters, Ω_c, Ω_Λ, and Ω_{tot} were graphed against $\log a$, for nine different values of γ_0. We denote the present-day values of Ω_b, Ω_c, Ω_r, and Ω_Λ as Ω_{b_0}, Ω_{c_0}, Ω_{r_0}, and Ω_{Λ_0} and define $\Omega_{m_0} \equiv \Omega_{b_0} + \Omega_{c_0} + \Omega_{r_0} = 0.3032$. Other present-day parameter

values are $h = 0.6821$, and $\Omega_{b_0}h^2 = 0.02234$, where

$$h \equiv \frac{H_0}{100} \tag{22}$$

is a parametrized form of the Hubble Rate. All of these parameter values are close to the current ΛCDM best-fit values. $\Omega_b h^2$ was used instead of the baryon density parameter Ω_b. Results are shown in Figure 6, Figure 7, and Figure 8.

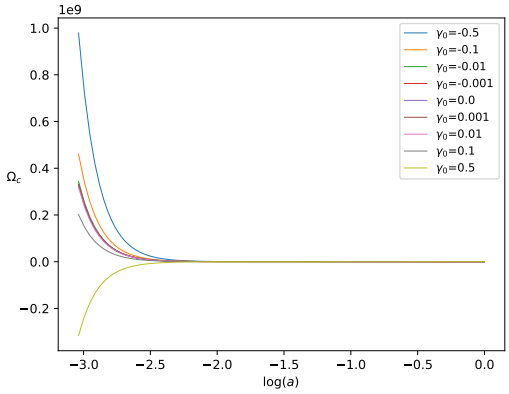

Figure 6: Graph of Ω_c vs. $\log(a)$ with IDS

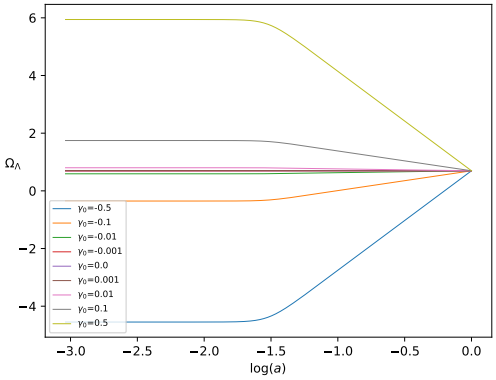

Figure 7: Graph of Ω_Λ vs. $\log(a)$ with IDS

$\gamma_0 = 0$ is equivalent to the ΛCDM model. By comparing different curves with the $\gamma_0 = 0$ curve, we could see that values of γ_0 as small as ± 0.001 are able to

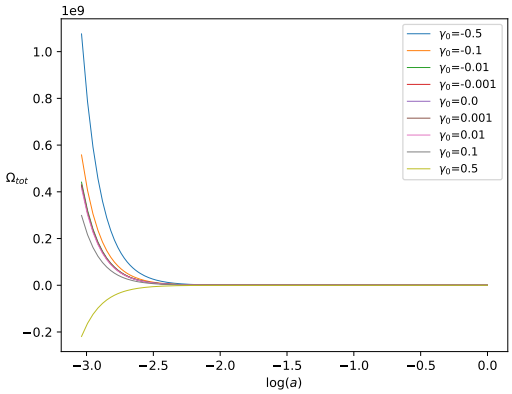

Figure 8: Graph of Ω_{tot} vs. $\log(a)$ with IDS

have noticeable impacts on the density parameter values.

To cross-check IDS parameter values, we propose and test an alternate IDS model with equation

$$\begin{aligned} \gamma(a) &= \frac{1+\tanh\left(k\left(\Omega_{c_1}-\Omega_c\right)\right)}{2} \\ Q &= \frac{3\Omega_c\left(1+\tanh\left(k\left(\Omega_{c_1}-\Omega_c\right)\right)\right)}{2a}. \end{aligned} \tag{23}$$

Here, k is a constant that could change the rate at which $\gamma(a)$ approaches 0 or 1. In our testing, we use the value $k = 0.00001$. Similar to with IDS, we make the approximation $\Omega_c/\Omega_{c_1} \approx a_1^3/a^3$ to reduce computation cost:

$$Q = \frac{3\Omega_c\left(1+\tanh\left(k\left(\frac{\Omega_{c_0}}{a_1^3}-\frac{\Omega_{c_0}}{a^3}\right)\right)\right)}{2a}. \tag{24}$$

2.2 Implementation

Markov chain Monte Carlo (MCMC) sampling with the Metropolis-Hastings algorithm was used to determine the best-fit values and probability distributions for present-day values Ω_{m_0}, $\Omega_{b_0}h^2$, and h. MCMC sampling works by finding the probability this set of values, evolved to early-universe times, describe the data, in the form of a likelihood function. To ensure the entire posterior gets sampled, the algorithm jumps to a new point in the parameter space with probability depending on this likelihood function. To carry out MCMC sampling, we use a

Python version[3] of the more commonly-used Fortran `CosmoMC`[4].

Our free parameters are Ω_{m_0}, $\Omega_{b_0}h^2$, h, and γ_0. Their sampling ranges are constrained from a variety of different measurements. Ω_{m_0} was set to vary between 0.15 and 0.50, around 50% on either side from the best-fit Planck 2018 result of 0.315 ± 0.007. The value of $\Omega_{b_0}h^2$ is constrained by primordial deuterium abundances found in BAO and is around 0.0220 ± 0.0005. Modern measurements of h all lie between 0.65 and 0.75; as a result, h was defined to vary in the interval $(0.60, 0.80)$ to allow for it to take values at and around all plausible values.

Since we know very little about γ_0, we let it vary between -1 and 1. This range was determined from experimentation; all values of gamma found had $|\gamma| \ll 1$.

$\Omega_{r_0}h^2$ was fixed because it is heavily constrained by the cosmic microwave background radiation temperature T_{cmb}. While Ω_{Λ_0} is not constrained by any observations, we still need $\Omega_{b_0} + \Omega_{c_0} + \Omega_{r_0} + \Omega_{\Lambda_0} = 1$; thus, Ω_{Λ_0} is constrained by the other parameters.

The present-day density parameter values could be converted to those at some other time by taking integrals over a of $d\Omega_{b,c,r,\Lambda}/da$; in the case of recombination, the integration range is from $a = 1$ to $a = 1/1090$. Unfortunately, it is very difficult to get a closed-form expression for this integral, so we use an ordinary differential equation (ODE) solver to integrate numerically. `odeint`, a `scipy` ODE solver that utilizes the LSODA method, was used. LSODA is versatile because it automatically switches between stiff[5] and non-stiff solvers based on the behaviour of the ODE. Other approximation methods are available, such as the second-order and fourth-order Runge-Kutta methods (RK23 and RK45) which are part of the `solve_ivp` solver, but in the end, LSODA was chosen for its superior speed.

Integrating numerically while doing MCMC sampling is quite computationally expensive. Being able to speed up each integral, even by a small amount, would allow for significant cuts to the total computing time, considering the large number of integrals involved. The adjustments of `odeint` error allowances `rtol`

[3] `https://github.com/slosar/april`

[4] `https://cosmologist.info/cosmomc`

[5] Stiff ODEs have slowly-varying solutions and corresponding solving algorithms need to have smaller step sizes.

and `atol` were attempted; however, it was found that changing one by an order of magnitude either way while fixing the other would cause the ODE solver to run around 30% more slowly, and that the default values of `rtol` and `atol` at $1.49012 \cdot 10^{-8}$ produced the best results.

We run the code with a variety of different datasets, for both ΛCDM and IDS. Each run was stopped when MCMC sampling had accepted 50000 parameter samples, a value where parameters are generally able to converge and after which and best-fit values barely change (this was found through experimentation). We use subsets of datasets within

- Baryon Oscillation Spectroscopic Survey (BOSS) Baryon Acoustic Oscillations, from distribution of quasars and galaxies[6] (BAO)
- Planck 2018 CMB data[7] (Planck)
- Type Ia Supernovae from the Sloan Dark Sky Survey II (SDSS-II), Super-Nova Legacy Survey (SNLS), and Hubble Space Telescope Cluster Supernova Survey (UnionSN) collaborations[8][9][10] (SN)
- Riess et al. (2019) measurements of the Hubble constant from Hubble Space Telescope Cepheid Variables[11], using Large Magellanic Cloud Cepheid Variables (H_0)

Out of the datasets used, only ones that contain Planck are able to constrain parameter values. Last but not least, to plot probability distributions and contour plots, we utilize the python package `GetDist`[12], which approximates MCMC samples with smooth curves. `GetDist` was also used to determine the parameter values at 68% CL, the value used to represent error bounds.

3 Results and Discussion

Best-fit values, error bounds, and χ^2 values for dataset combinations, for both ΛCDM and IDS, are shown in Table 1. IDS reduces χ^2 values for all datasets

[6] `http://www.sdss3.org/surveys/boss.php`
[7] `https://www.cosmos.esa.int/web/planck`
[8] `https://www.sdss.org/dr12/data_access/supernovae`
[9] `http://irfu.cea.fr/en/Phocea/Vie_des_labos/Ast/ast_technique.php?id_ast=2289`
[10] `http://supernova.lbl.gov/Union`
[11] `https://archive.eso.org/cms/hubble-space-telescope-data.html`
[12] `https://getdist.readthedocs.io`

Model	Datasets	h	Ω_{m_0}	$\Omega_{b_0}h^2$	γ_0	χ^2
ΛCDM	Planck+SN	0.688 ± 0.013	0.295 ± 0.016	0.02243 ± 0.00033	N/A	27.2551
ΛCDM	BAO+Planck	0.6814 ± 0.0066	0.3031 ± 0.0082	0.02232 ± 0.00027	N/A	5.12304
ΛCDM	BAO+Planck+SN	0.6818 ± 0.0063	0.3025 ± 0.0078	0.02232 ± 0.00027	N/A	32.4011
ΛCDM	Planck+H_0	0.715 ± 0.010	0.263 ± 0.011	0.02297 ± 0.00029	N/A	3.19027
ΛCDM	Planck+SN+H_0	0.7105 ± 0.0093	0.268 ± 0.010	0.02289 ± 0.00028	N/A	31.1657
ΛCDM	BAO+Planck+H_0	0.6922 ± 0.0061	0.2902 ± 0.0073	0.02260 ± 0.00026	N/A	12.2886
ΛCDM	BAO+Planck+SN+H_0	0.6918 ± 0.0058	0.2907 ± 0.0070	0.02259 ± 0.00026	N/A	39.5645
IDS	Planck+SN	$0.686^{+0.028}_{-0.033}$	0.297 ± 0.026	0.02244 ± 0.00036	-0.0005 ± 0.0059	27.2689
IDS	BAO+Planck	0.6789 ± 0.0077	0.3022 ± 0.0083	0.02245 ± 0.00035	-0.0016 ± 0.0027	4.96449
IDS	BAO+Planck+SN	0.6793 ± 0.0076	0.3019 ± 0.0081	0.02244 ± 0.00035	-0.0016 ± 0.0027	32.2365
IDS	Planck+H_0	0.739 ± 0.014	0.255 ± 0.011	0.02247 ± 0.00036	0.0078 ± 0.0031	0.010435
IDS	Planck+SN+H_0	0.731 ± 0.013	0.262 ± 0.010	0.02240 ± 0.00036	0.0073 ± 0.0031	28.4602
IDS	BAO+Planck+H_0	0.6937 ± 0.0071	0.2912 ± 0.0076	0.02247 ± 0.00035	0.0013 ± 0.0026	12.1982
IDS	BAO+Planck+SN+H_0	0.6934 ± 0.0069	0.2915 ± 0.0073	0.02248 ± 0.00035	0.0012 ± 0.0026	39.4632

Table 1: Best-fit values, error bounds, and χ^2 values for different model-dataset combinations

except for Planck+SN. Two datasets, H_0 and BAO particularly influence the parameter best-fit values.

The inclusion of H_0 results in positive γ_0, i.e. decreasing dark energy density. Furthermore, the modified model, when and only when run with datasets that include H_0, demonstrates best-fit values of h higher than the ΛCDM model with corresponding datasets. In other words, H_0 is able to increase goodness-of-fit and decrease Hubble rate tensions. This is partially a consequence of the nature of the dataset: H_0 directly uses Hubble rate data points from Riess et al. (2019), the dataset with which ΛCDM directly demonstrates tensions. As a result, this result does not directly show that IDS reduces Hubble rate tensions given our current understanding of the universe (when run with datasets without H_0, IDS increased Hubble rate tensions).

BAO appears to limit the change in parameter best-fit values: datasets that include BAO have best-fit values of h that vary by a maximum of 0.0025 between models. This might be the case because BAO and Planck CMB measure the same attributes of CMB from very low ($z = 2$) and high ($z = 1090$) redshifts, respectively; in addition, two of the three parameters that describe BAO, sound horizon at decoupling r_d and density parameter $\Omega_m h^2$, are well-constrained by CMB, which leaves little room for the third parameter, h, to change value. Due to the constraint of both $\Omega_m h^2$ and h of BAO, Ω_m is more constrained with datasets that contain BAO.

Probability distributions and contour plots of different model-dataset combinations are shown in Figure 9,Figure 10,Figure 11, and Figure 12. Datasets within each model are grouped into graphs by whether they contain H_0 due

to the large influence of H_0 on best-fit values. The datasets BAO+Planck and BAO+Planck+H_0 are omitted from plots due to the similarity between their results and those of BAO+Planck+SN and BAO+Planck+SN+H_0.

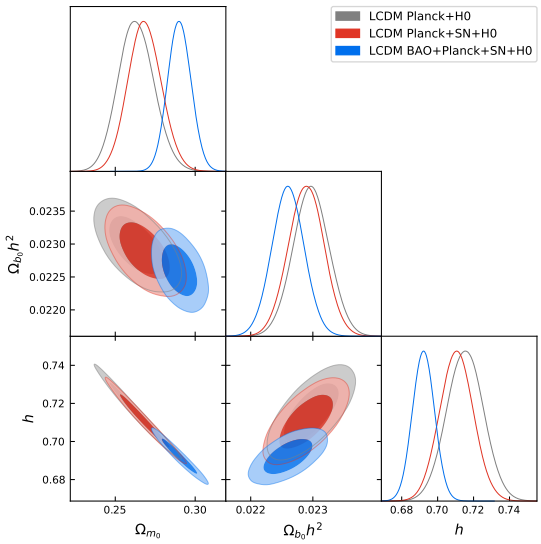

Figure 9: LCDM plots for datasets with H_0. BAO probability distributions noticeably differ from non-BAO distributions. All best-fit h values are higher than those of corresponding datasets without H_0 due to the nature of the H_0 dataset.

Ratios of h values between different model-dataset combinations and ΛCDM BBAO+Planck+SN+H_0 were plotted against $\log(z)$, as shown in Figure 13 and Figure 14. IDS datasets and their corresponding ΛCDM datasets are plotted on the same graph; the datasets are again divided according to whether they contain H_0.

We define the interaction switch-on redshift z_{on} as the redshift that satisfies $\gamma(a(z_{\text{on}}))/\gamma_0 = 0.1$, where $a(z_{\text{on}}) \equiv 1/(z_{\text{on}}+1)$, i.e. it is the redshift after which the interaction starts to become significant. In the modified model, $z_{on} \approx 75.7$. The line $\log(z) = \log(z_{\text{on}})$ was also plotted to indicate approximately when the interaction starts.

The graphs show that due to the positive γ_0 values of datasets with H_0, dark energy density is comparatively larger at later times, leading to larger h values. IDS graphs reach extrema at values of z close to z_{on}. The proximity of the

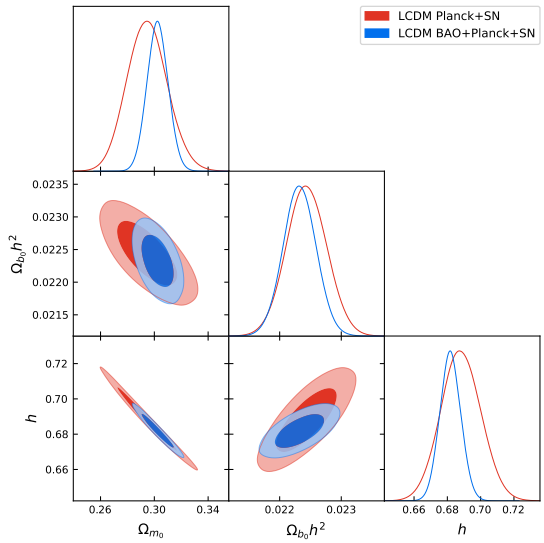

Figure 10: LCDM plots for datasets without H_0. All best fit values for h are under 0.70.

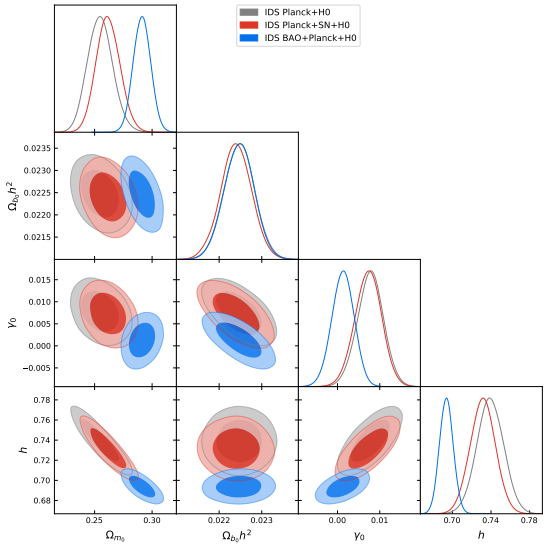

Figure 11: IDS plots for datasets with H_0. Values for H are higher than corresponding LCDM values. Planck+H_0 and Planck+SN+H_0 have especially high h values over 0.730.

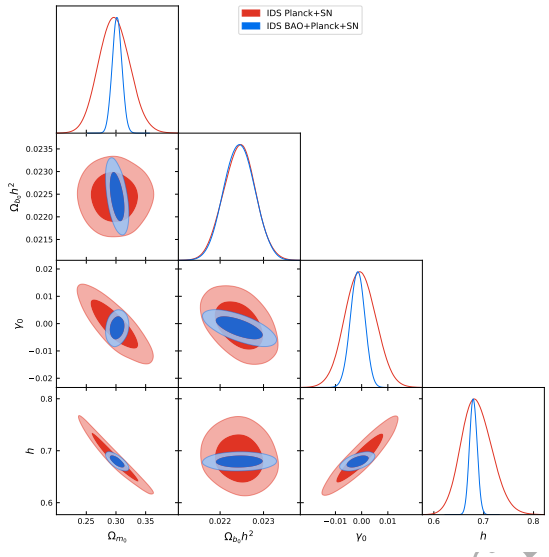

Figure 12: IDS plots for datasets without H_0. Best-fit values for h are all slightly lower than corresponding LCDM values.

ΛCDM Planck+SN+H_0 curve with a horizontal line again shows that datasets with BAO cause modified plots to deviate very little from corresponding LCDM plots.

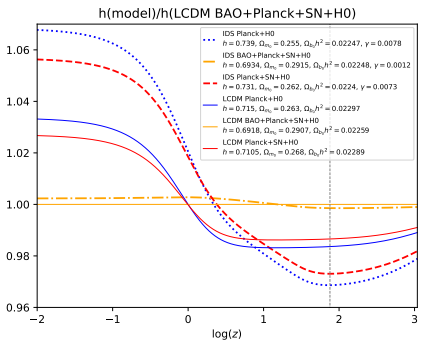

Figure 13: Relative H vs. log(z) plots for datasets with H_0

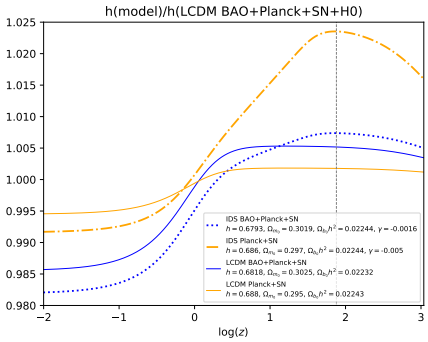

Figure 14: Relative H vs. log(z) plots for datasets without H_0

MCMC on the dataset Planck+SN+H_0 was run with variations of IDS with four other values of z_{on}, with results shown in Table 2. Values of z_{on} are listed

in the table. The middle two values of z_{on} lie in the matter-dominated era; the smallest and largest z_{on} values lie in the dark energy and radiation dominated eras, respectively.

Q/γ_0	z_{on}	h	Ω_{m_0}	$\Omega_{b_0}h^2$	γ_0	χ^2
$\frac{1+\tanh\ln(a^3\cdot 7.3173\cdot 10^9))}{2}$	2740	0.732 ± 0.013	0.262 ± 0.010	0.02240 ± 0.00035	0.0066 ± 0.0028	28.4493
$\frac{1+\tanh(\ln(a^3\cdot 5000^{3/2}))}{2}$	100.9	0.731 ± 0.013	0.262 ± 0.010	0.02240 ± 0.00036	0.0076 ± 0.0032	28.4576
$\frac{1+\tanh(\ln(a^3\cdot 500^{3/2}))}{2}$	31.2	0.731 ± 0.013	0.262 ± 0.010	0.02239 ± 0.00036	0.0069 ± 0.0029	28.4594
$\frac{1+\tanh(\ln(a^3\cdot 9/8))}{2}$	0.6	0.730 ± 0.0123	0.263 ± 0.010	0.02240 ± 0.00035	0.097 ± 0.042	28.6929

Table 2: Best-fit values, error bounds, and χ^2 values for variations of the modified model with different values of z_{on}, using the dataset Planck+SN+H_0

Relative h vs. $\log(z)$ plots for modified IDS models with different values z_{on} were also generated, as shown in Figure 15. Again, the reference model-dataset combination for h is ΛCDM BAO+Planck+SN+H_0. ΛCDM Planck+SN+H_0 is also plotted; the similarity between its curve and a horizontal line shows that BAO alters results minimally when compared to other datasets. The minima of the IDS and modified IDS graphs all occur at their corresponding z_{on} values. Furthermore, the larger the z_{on} value, the smaller the h ratio at minima.

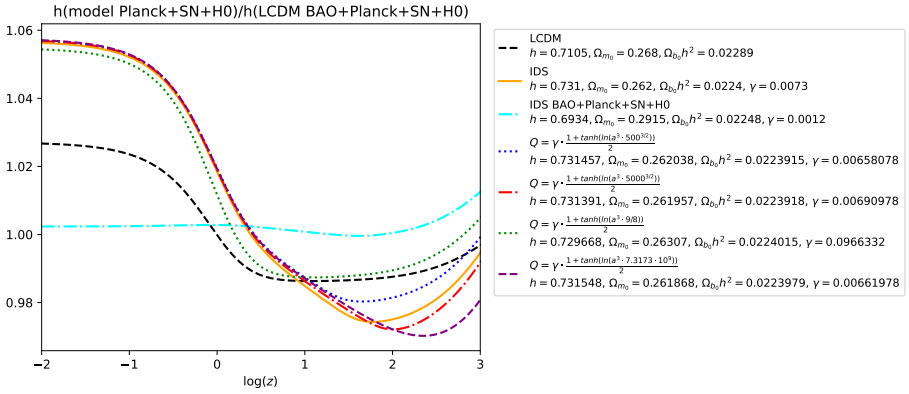

Figure 15: Comparison of H vs. $\log(z)$ plots for different values of z_{on}

Values of $t \cdot H$ were plotted against $\log(a)$ for datasets with and without H_0. Since

$$a \propto t^{2/(3+3w)}, \tag{25}$$

where w is the equation of state constant, and $H = \dot{a}/a$, $t \cdot H$ would approximately equal 1/2 and 2/3 in the radiation and matter dominated eras, respec-

tively. It could be seen in Figure 16 and Figure 17 that values for $t \cdot H$ equal to $1/2$ at small values of a and reaches $2/3$ at a value of $\log(a)$ between $z = 2740$ and $z = 0.3$, the radiation-matter and matter-dark energy equality redshifts. The dataset Planck+H_0 was omitted due to its plot's indistinguishability with that of Planck+SN+H_0.

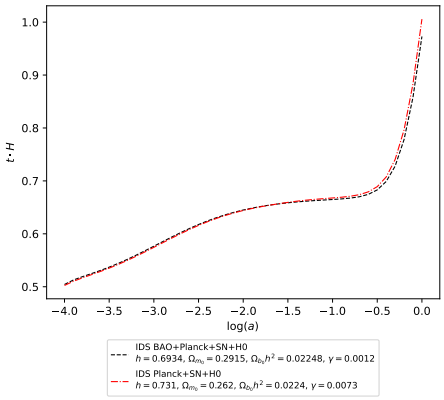

Figure 16: $t \cdot H(a)$ vs. $\log(a)$ plots for datasets with H_0

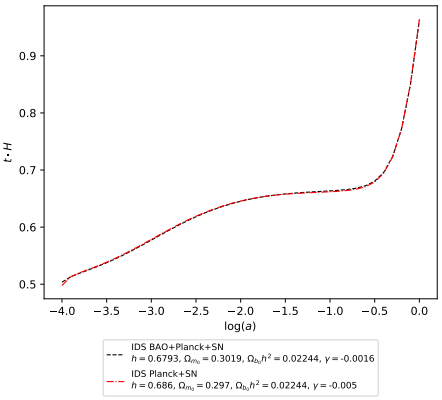

Figure 17: $t \cdot H(a)$ vs. $\log(a)$ plots for datasets without H_0

The alternate version of IDS with equation $\gamma(a) = \frac{1+\tanh\left(k\left(\Omega_{c_1} - \Omega_c\right)\right)}{2}$ was also run with all datasets; however, its results are negligibly close to those of IDS and are thus omitted.

4 Conclusion

The Interacting Dark Sector model decreased Hubble rate tensions for datasets containing H_0. However, Hubble rate tensions increased by a smaller amount for datasets without H_0. Since H_0 is taken directly from Riess et al. (2019) results, IDS is unlikely to solve the Hubble tension with our current understanding of the universe. The positive value of γ and increased h in runs containing the dataset H_0 gives some degree of support for a relationship between decaying dark energy and lower Hubble rate tensions. If evidence of decreasing dark energy density is ever found, models similar to IDS are a possible solution to the Hubble tension.

Acknowledgements

First, I would like to thank my research supervisor Prof. Levon Pogosian of Simon Fraser University for all his support in this project. Without his willingness to take in a high school student, his patience while I was learning background materials, and his knowledgable guidance in both theory and computation, this project wouldn't be where it is today. I also would like to thank Hamid Mirpoorian, SFU physics MSc candidate, for his helpful suggestions about the process of research.

References

[1] Aubourg, E., Bailey, S., Bautista, J. E., et al. (2015). Cosmological implications of baryon acoustic oscillation (bao) measurements. *Physical Review D*, 92(12).

[2] Bocquet, S., Dietrich, J. P., Schrabback, T., et al. (2019). Cluster cosmology constraints from the 2500 deg^2 spt-sz survey: Inclusion of weak gravitational lensing data from magellan and the hubble space telescope. *The Astrophysical Journal*, 878(1).

[3] Carroll, B. W. and Ostlie, D. A. (2017). *An Introduction to Modern Astrophysics*. Cambridge University Press.

[4] Carroll, S. M. (2019). *Spacetime and Geometry: An Introduction to General Relativity*. Cambridge University Press.

[5] D'Inverno, R. (2008). *Introducing Einstein's Relativity*. Academic Press.

[6] Dodelson, S. (2003). *Modern Cosmology*. Academic Press.

[7] Hinshaw, G., Larson, D., Komatsu, E., et al. (2013). Nine-year wilkinson microwave anisotropy probe (wmap) observations: Cosmological parameter results. *The Astrophysical Journal Supplement Series*, 208(2).

[8] Huang, C. D., Riess, A. G., Yuan, W., et al. (2020). Hubble space telescope observations of mira variables in the sn ia host ngc 1559: An alternative candle to measure the hubble constant. *The Astrophysical Journal*, 889(1).

[9] Lahav, O. and Liddle, A. R. (2017). The cosmological parameters. *Review of Particle Physics*.

[10] Liddle, A. R. (2015). *An Introduction to Modern Cosmology*. John Wiley and Sons, Inc.

[11] Mandolesi, N., Burigana, C., Gruppuso, A., et al. (2020). The planck mission: Recent results, cosmological and fundamental physics perspectives. *Astronomy and Astrophysics*, 641.

[12] Miller, D. R. (2019). Dark sector cosmic fluid interactions as a solution to the observed disagreement in measurements of the hubble expansion rate. Honours undergraduate thesis, Simon Fraser University.

[13] Olive, K. A. and Peacock, J. A. (2019). Big-bang cosmology. *Review of Particle Physics*.

[14] Pesce, D. W., Braatz, J. A., Reid, M. J., et al. (2020). The megamaser cosmology project. xiii. combined hubble constant constraints. *The Astrophysical Journal Letters*, 891(1).

[15] Pogosian, L. (2017). Expanding isotropic and homogenous universe. Lecture notes.

[16] Riess, A. G., Casertano, S., Yuan, W., et al. (2019). Large magellanic cloud cepheid standards provide a 1% foundation for the determination of the hubble constant and stronger evidence for physics beyond Λcdm. *The Astrophysical Journal*, 876(1).

[17] Riess, A. G., Filippenko, A. V., Challis, P., et al. (1998). Observational evidence from supernovae for an accelerating universe and a cosmological constant. *The Astronomical Journal*, 116(3).

[18] Risalti, G. and Lusso, E. (2019). Cosmological constraints from the hubble diagram of quasars at high redshifts. *Nature Astronomy*, 3:272–277.

[19] Ryden, B. S. (2017). *Introduction to Cosmology*. Cambridge University Press.

[20] von Marttens, R., Casarini, L., Mota, D. F., et al. (2019). Cosmological constraints on parametrized interacting dark energy. *Physics of the Dark Universe*, 23.

[21] Wong, K. C., Suyu, S. H., Chen, G. C.-F., et al. (2020). H0licow xiii. a 2.4% measurement of h_0 from lensed quasars: 5.3σ tension between early and late-universe probes. *Monthly Notices of the Royal Astronomical Society, stz3094*.